IJRCS

International Journal of Robotics and Control Systems
Vol. 6, No. 1, 2026, pp. 92–114
ISSN 2775-2658
http://pubs2.ascee.org/index.php/ijrcs

ASCEE

Safe Periodic Tracking via a Repetitive Controller with Control Barrier Function Constraints: A Servomotor Simulation Study

Ronald Edward [a,1], Rahmadwati [a,2,*], M. Aziz Muslim [a,3], Akif Rahmatillah [b,4], Edi Kurniawan [c,5,*]

[a] Department of Electrical Engineering, Universitas Brawijaya, Malang, Indonesia
[b] Biomedical Engineering Study Program, Universitas Airlangga, Surabaya, Indonesia
[c] Research Center for Photonics, National Research and Innovation Agency, South Tangerang, Indonesia
[1] ronaldedward999@student.ub.ac.id; [2] rahma@ub.ac.id; [3] muh_aziz@ub.ac.id; [4] akif-r@fst.unair.ac.id;
[5] edik004@brin.go.id
[*] Corresponding Authors

ARTICLE INFO

Article History
Received October 27, 2025
Revised November 30, 2025
Accepted December 25, 2025

Keywords
Safe Periodic Tracking;
Repetitive Controller;
Exponential Control Barrier Function;
Quadratic Programming;
Servomotor Simulation

ABSTRACT

In many control applications, achieving precise tracking and rejecting periodic disturbances remain persistent challenges. A widely adopted solution is repetitive control (RC), which provides excellent steady-state performance for periodic reference tracking but often exhibits large overshoots during transients and offers only asymptotic stability guarantees. To overcome these limitations, this study integrates a Control Barrier Function (CBF) into an output-feedback RC framework to enforce safety while maintaining tracking accuracy. In the proposed structure, the CBF operates as a safety filter that modifies the RC–PD control input only when needed to prevent potential violations of predefined output states. This ensures that system trajectories remain within a prescribed safe region throughout operation. The framework is validated through a servomotor simulation study, including a case with periodic disturbance to demonstrate consistent tracking behavior under non-nominal operating condition. The simulation results show that the RC–CBF controller eliminates overshoot, ensuring transient safety while preserving the key benefits of RC in achieving accurate steady-state periodic tracking. Although the integration of the CBF introduces a slight increase in steady-state error compared with standalone RC, the error remains negligible for all tested conditions. By contrast, a PD controller with or without a CBF yields safer transients than standalone RC but does not achieve the steady-state accuracy of RC-based methods. Overall, combining RC with CBF offers a practical way to enforce transient safety while preserving accurate periodic tracking, making the approach promising for precise reference tracking and disturbance rejection in industrial applications.

1. Introduction

In many control applications, accurate tracking and rejection of periodic signals remain a common challenge. A widely adopted solution is repetitive control (RC), first proposed by Inoue et al. [1]. RC concept was originated by the Internal Model Principle (IMP) developed in [2], which enables periodic reference tracking and disturbance rejection with minimal steady-state error [3]. Compared to classical control schemes such as PID, RC provides superior performance because it learns and

reuses the repeating components of a signal as feedforward input [4]. This is achieved by inserting a one-period delay in the feedback loop, storing the error from the previous period, and using it to correct the next cycle. RC methods are generally classified into two categories: state-feedback RC and output-feedback RC. State-feedback RC is designed in the state-space framework and is typically synthesized in the continuous-time domain [5], whereas output-feedback RC is formulated using transfer-function models in the discrete-time frequency domain [6]. In the discrete-time framework, RC is usually constructed from two components: the internal model and a compensator. The internal model generates the periodic pattern using a delay whose length matches the period of the reference, thereby enabling tracking or rejection of periodic signals. The compensator, often viewed as a learning function, ensures closed-loop stability and determines the convergence rate of the overall RC system.

RC has demonstrated effectiveness across diverse applications involving periodic signal tracking and rejection, including functional electrical stimulation (FES) [7]–[10], pulse width modulation (PWM) converters [11]–[14], active power filters [15], and flexible robotic joints [16]–[18]. Recent developments in RC-related approaches have been surveyed across numerous studies [19]–[26]. For instance, [19] proposed a novel design methodology for the development of a compensator for discrete-time high-order RC (HORC) systems. The compensator is derived by fulfilling the HORC stability criterion, which is necessary for formulating an objective function that addresses the compensator design challenge as an optimization problem. The method applies to both minimum-phase and non-minimum-phase systems. In [20], preview RC with an equivalent-input-disturbance (EID) estimator for continuous-time systems was introduced by converting the one-period delay into a delay-free form and using a linear quadratic regulator (LQR) to synthesize the controller, thereby improving periodic tracking and rejection of unknown disturbances. A model-reference RC combined with HORC was proposed in [21] for a class of linear systems to track time-varying references and reject uncertain periodic disturbances. Furthermore, [22] presented a general multi-frequency RC algorithm for power converters that can track periodic references and reject periodic disturbances, including multi-frequency components.

Building on these advances, several researchers have further extended the RC framework to address more complex scenarios. For example, the advancement of RC formulations to enhance direct force control in quasi-periodic human–robot interaction was presented in [23], where a zero-force controller was assessed via simulations and bench-top experiments against a passive proportional baseline. In addition, [24] introduced a discrete-time RC with a fractional-delay internal model that allows for more accurate tracking, especially when the delay duration is not an integer. Subsequently, [25] proposed a novel disturbance-rejection framework for RC systems that addresses unknown dynamics by explicitly aligning the EID compensation with the estimated EID, constructing a minimal loop that couples the EID estimate, the output-error signal, and the compensation signal. Moreover, [26] developed an algorithm consisting of a fractional-delay RC scheme combined with a nonlinear control method, namely the sliding mode control technique. In this approach, the fractional-delay RC is utilized for trajectory tracking and disturbance rejection to enhance steady-state accuracy, while sliding mode control improves the transient response of the RC system and ensures robustness against parametric uncertainties.

Beyond these developments, RC has been applied to a broad spectrum of system classes, including single-input single-output (SISO) systems [27]–[30], nonlinear SISO systems [31]–[34], and multi-input multi-output (MIMO) systems [35]–[40]. While RC demonstrates excellent performance in tracking and rejecting periodic signals across these diverse systems, several inherent limitations remain. One major concern is the potential for excessively large control signals, particularly during the initial learning phase or when the reference or disturbance varies unpredictably. In its effort to rapidly suppress periodic errors, the controller often generates high-amplitude control actions, which can lead to larger overshoots compared to conventional controllers, especially during transient phases of each cycle [41]. Furthermore, RC guarantees only asymptotic stability in periodic tracking and

does not provide formal safety assurances for the plant output. In the absence of explicit constraint-handling mechanisms—such as actuator saturation or state/output limits—transient responses may violate safety bounds even though convergence is ultimately achieved. Accordingly, the integration of a safety framework is essential to ensure that the RC control input and plant output remain within acceptable limits.

Accordingly, one control approach that not only guarantees stability but also ensures system safety throughout the control process is the Control Barrier Function (CBF). A CBF defines a safe set in the system's state space and keeps the system within it by imposing barrier-based constraints on the control input [42]–[44]. It offers a simple yet effective means to augment controllers in applications that must enforce safety performance. Conceptually, a CBF acts as a supervisor (safety filter) that modifies the control command whenever a potential safety violation is detected [42], [45]. Moreover, CBFs offer a rigorous framework for enforcing safety in control systems while accommodating performance objectives through integration with nominal or Control Lyapunov Function (CLF)-based controllers [46]. By enforcing barrier-based constraints on states and inputs, CBFs restrict system trajectories to a prescribed safe set and certify forward invariance, even in the presence of uncertainty and external disturbances [47]. In practice, CBFs synthesize safety feedback so that any trajectory starting in an admissible initial set remains within the safe set and never enters its complement (the unsafe region), mirroring the relationship between Lyapunov functions and CLFs [48], [49]. A common approach to designing a CBF is to first specify hard constraints and then construct a function that guarantees forward invariance of a prescribed safety set, which is particularly effective for simple linear constraints [50].

Because of their strong safety guarantees, CBF frameworks have been successfully applied to a wide range of control problems, including robotics applications [51]–[54], adaptive cruise control [55]–[58], permanent magnet (PM) motor control [59]–[62], and dynamic balancing of Segways [63]–[65]. Several studies provide comprehensive theoretical and experimental evidence that barrier-based constraints can enforce forward invariance of prescribed safe sets, accommodate model uncertainties and disturbances through real-time optimization, and be seamlessly integrated with nominal controllers—such as model predictive control, iterative learning control, CLF-based quadratic programming (QP), and sliding mode control—to maintain tracking performance while guaranteeing safety [57], [58], [66]–[70]. For instance, [57], [58] introduced a barrier-function formulation that implies forward invariance and demonstrated how CBF can be unified with CLF in a QP to balance performance and safety. In [66], it was shown that a CBF can be implemented as a standalone safety mechanism that minimally modifies the nominal control input to maintain system safety. To address restrictions with high relative-degree constraints, [67] developed the exponential CBF. Subsequently, High-Order CBFs (HOCBFs) were introduced in [68], generalizing CBFs to arbitrary relative degrees, providing Lyapunov-like conditions that ensure forward invariance of safety sets, and improving QP feasibility through penalty and parameterization methods. The framework in [69] extended CBFs to uncertain nonlinear systems with actuator saturation, eliminating the need for prior disturbance bounds, enforcing prescribed tracking-error limits, and reducing chattering in conventional sliding mode control. Furthermore, [70] presented a CBF combined with model-free adaptive iterative learning control to guarantee safety via QP constraints while handling system uncertainties. While RC and CBF have been widely studied, to the best of our knowledge the specific learning–projection interaction in safety-critical repetitive tracking has not been systematically characterized.

In safe periodic tracking, RC attains high steady-state accuracy by learning from cycle-to-cycle tracking error, yet it lacks formal safety guarantees and can require large control efforts during transients. CBFs complement RC by enforcing state and input constraints through an optimization-based safety filter that projects the nominal control input onto a constraint-admissible set. Such a safety-critical repetitive tracking capability is particularly relevant for industrial electromechanical systems that operate under periodic motion, such as servo-driven positioning stages, flexible robotic joints, and

machinery requiring active vibration compensation. In these applications, large transient overshoots or violations of position and input constraints can lead to degraded product quality, accelerated mechanical wear, or even unsafe operating conditions, making an RC–CBF framework especially attractive.

Therefore, this study aims to integrate a Control Barrier Function (CBF) with Repetitive Control (RC) to overcome the inherent limitations of conventional RC and analyzes their interaction to derive a practical architecture that retains high tracking accuracy while guarantee enforcing safety. In particular, RC often suffers from large control efforts during transients and provides only asymptotic stability without formal safety guarantees. To address these issues, we propose a repetitive proportional–derivative controller augmented with a control barrier function (RCPD-CBF) for accurate and safe periodic signal tracking. The proposed approach not only ensures a small steady-state tracking error but also enforces safety by imposing state and input constraints. In the integrated architecture, the RC–PD serves as the nominal controller responsible for tracking and rejecting periodic components, while the CBF acts as a real-time safety filter that minimally adjusts the nominal control input, for instance, through a quadratic program that prioritizes constraint satisfaction over tracking accuracy, whenever the system is at risk of violating safety limits. This work's primary contributions are summarized as follows:

1. A novel and systematic integration of RCPD and CBF is developed and analyzed for a single-input single-output (SISO) linear servomotor system, combining their complementary strengths to achieve accurate periodic tracking while enforcing safety constraints during transients and maintaining tracking precision at steady state.
2. The inclusion of the CBF in the nominal RC controller ensures boundedness of both the system states and the control input through forward-invariance conditions on prescribed state and input constraints, in addition to the asymptotic convergence properties of RC.
3. The effectiveness of the proposed RCPD augmented with a CBF is validated through simulations both in a disturbance-free case and under a disturbance, demonstrating superior periodic-tracking performance and enhanced safety compared with RCPD, PD-CBF, and standalone PD controllers.

The remainder of this paper is organized as follows. Section 2 outlines the proposed methodology, including the plant modeling, standalone output-feedback RC design, standalone CBF design, and the development of the integrated RC–CBF strategy. Section 3 presents the simulation results, comparative analysis, and discussion, while Section 4 concludes the study.

2. Method

2.1. Plant Modelling

In this study, a servomotor system is employed as the plant model [71]. The motor dynamics are represented as a linear system relating the armature voltage $v_m(t)$ (input) to the load–shaft speed $\omega_\ell(t)$ (output). By lumping the motor, gear, and load effects into equivalent inertia and damping terms, the governing equation can be expressed as

$$J_{eq}\,\dot{\omega}_\ell(t) + B_{eq}\,\omega_\ell(t) = A_m\,v_m(t), \tag{1}$$

Where J_{eq} is the equivalent inertia, B_{eq} the viscous damping coefficient, and A_m the actuator gain capturing the electromechanical coupling, $v_m(t)$ is an input voltage and $\omega_\ell(t)$ is an angular velocity. Applying the Laplace transform of (1) under zero initial conditions yields the transfer function

$$\frac{\omega_\ell(s)}{V_m(s)} = \frac{A_m}{J_{eq}s + B_{eq}} = \frac{K}{\tau s + 1}, \tag{2}$$

Where $K = \frac{A_m}{B_{eq}}$ and $\tau = \frac{J_{eq}}{B_{eq}}$ represent the steady-state gain and time constant, respectively. Considering the angular position $\theta(t)$ as the output, an additional integration gives the voltage-to-position

transfer function

$$\frac{\theta(s)}{V_m(s)} = \frac{X(s)}{U(s)} = \frac{K}{s(\tau s + 1)}. \tag{3}$$

For simplicity, the Laplace-domain input and output are represented as $U(s)$ for the input voltage and $X(s)$ for the angular position. Applying the inverse Laplace transform to (3) yields the second-order differential equation. Under zero initial conditions for $x(t)$ and $\dot{x}(t)$, the system dynamics become:

$$\ddot{x}(t) = -\frac{1}{\tau}\dot{x}(t) + \frac{K}{\tau}u(t), \tag{4}$$

Where $x(t)$ denotes the angular position, $\dot{x}(t)$ the angular velocity, $\ddot{x}(t)$ the angular acceleration, and $u(t)$ the input voltage in the time domain. The corresponding state-space representation of the plant is therefore

$$\dot{\mathbf{x}}(t) = \underbrace{\begin{bmatrix} 0 & 1 \\ 0 & -\frac{1}{\tau} \end{bmatrix}}_{\mathbf{A}} \mathbf{x}(t) + \underbrace{\begin{bmatrix} 0 \\ \frac{K}{\tau} \end{bmatrix}}_{\mathbf{B}} u(t), \qquad y(t) = \underbrace{\begin{bmatrix} 1 & 0 \end{bmatrix}}_{\mathbf{C}} \mathbf{x}(t), \tag{5}$$

Where $\mathbf{x}(t) = [x_1(t)\ x_2(t)]^\top = [x(t)\ \dot{x}(t)]^\top = [\theta(t)\ \omega_\ell(t)]^\top$ is the state vector, $\mathbf{A}$ is a system matrix, $\mathbf{B}$ is an input matrix, and $\mathbf{C}$ is an output matrix. The transfer function (3) and state-space model (5) represent the final plant model used in this work. Finally, the block diagram of the open-loop plant model can also be illustrated in Fig. 1.

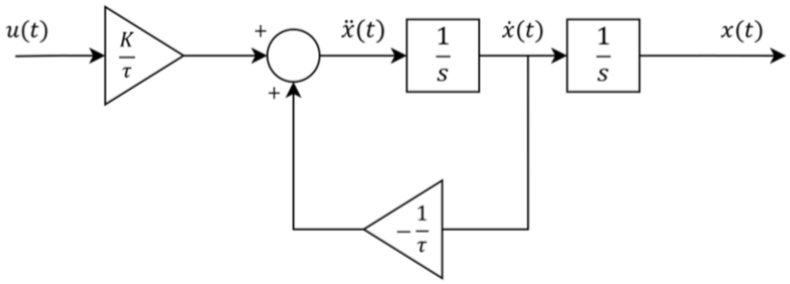

Fig. 1. Block diagram of the open-loop servomotor plant model illustrating the relationship between the input voltage $u(t)$ and the angular position $x(t)$

2.2. Output-Feedback RC

The structure of the output-feedback repetitive controller (RC) is illustrated in Fig. 2, where the RC is implemented in a plug-in configuration with a conventional controller $C(z)$. The term output-feedback RC refers to a configuration in which only the measured output state is used for feedback to the RC. The RC-based system aims to achieve accurate tracking of a periodic reference signal $r(k)$, where $r(k)$ denotes the desired trajectory to be followed. The tracking error $e(k)$ is defined as the difference between the reference input and the plant output, expressed as

$$e(k) = r(k) - y(k), \tag{6}$$

Where $y(k)$ represents the plant output. Based on Fig. 2, $P(z)$ denotes the discrete-time plant model, $C(z)$ represents the conventional controller, $I(z)$ is the internal model of the RC, and $L(z)$ is the RC compensator.

The signal $u_{rc}(k)$ corresponds to the control signal generated by the plug-in RC. The transfer function of the plug-in RC can be expressed as

$$\frac{U_{rc}(z)}{E(z)} = I(z)L(z), \tag{7}$$

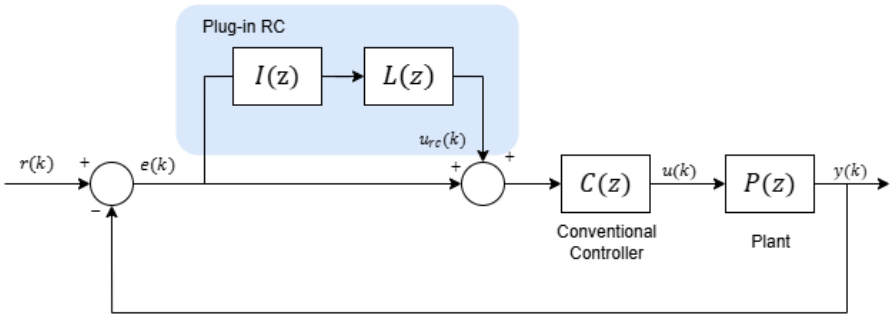

Fig. 2. Closed-loop system block diagram incorporating the output-feedback RC

Where $E(z)$ is the z-transform of the tracking error.

The essential design task in the plug-in RC structure is to determine the internal model $I(z)$ based on the internal model principle (IMP) and to design a stabilizing compensator $L(z)$. The discrete-time internal model is formulated as

$$I(z) = \frac{Q(z)z^{-N}}{1 - Q(z)z^{-N}}, \tag{8}$$

Where $N = T_r/T_s$ is the number of samples per reference period, T_s is the sampling period, and $Q(z)$ is a low-pass filter. In this study, $Q(z)$ is selected as a zero-phase low-pass moving-average filter defined by

$$Q(z) = q_0 + \sum_{j=1}^{n} q_j (z^j + z^{-j}), \tag{9}$$

Where n denotes the filter order and the coefficients $q_0, q_1, \ldots, q_n$ satisfy

$$q_0 + 2\sum_{j=1}^{n} q_j = 1. \tag{10}$$

The filter structure in (9) and condition in (10) ensures that the Q-filter provides unity gain within the tracking bandwidth and maintains zero phase across all frequencies.

The compensator $L(z)$ plays a crucial role in ensuring closed-loop stability when the plug-in RC is employed. For the closed-loop configuration shown in Fig. 2, the stabilized plant is defined as

$$P_s(z) = \frac{C(z)P(z)}{1 + C(z)P(z)}, \tag{11}$$

Where $C(z)$ is a conventional feedback controller, such as a proportional–derivative (PD) controller. In this work, the stabilizing compensator $L(z)$ is chosen based on the general stability conditions of plug-in RC, namely that (i) $P_s(z)$ is internally stable and (ii) the following norm holds:

$$\left\| \left(1 - L(z)P_s(z)\right)Q(z) \right\|_\infty < 1. \tag{12}$$

From (12), it is evident that $L(z)$ is designed to cancel both the magnitude and phase of $P_s(z)$ within the tracking bandwidth, achieving ideal compensation when

$$L(z) = \frac{1}{P_s(z)}. \tag{13}$$

This choice requires that $P_s(z)$ be stable and minimum phase so that $P_s^{-1}(z)$ does not introduce unstable poles. In cases where $P_s(z)$ exhibits non–minimum–phase characteristics, alternative compensator designs may be adopted, such as those proposed in [72].

Although the ideal choice (13) may lead to an improper transfer function, its implementation remains practical. Let d_N and d_D denote the numerator and denominator degrees of $L(z)$, respectively, and define $n_L = d_N - d_D \geq 0$. The compensator is then realized as a proper block by multiplying $L(z)$ with a pure delay z^{-n_L} in the controller, while the factor z^{n_L} is absorbed into the internal model. Substituting this decomposition into (7) and (8) yields the final form of the output–feedback RC:

$$U_{rc}(z) = \left(\frac{Q(z)\, z^{-N+n_L}}{1 - Q(z)\, z^{-N}} \right) \left(z^{-n_L} L(z) \right) E(z), \tag{14}$$

Where $Q(z)$ and $L(z)$ are designed according to (9) and (13), respectively, and the implemented compensator $z^{-n_L} L(z)$ is proper and suitable for realization.

2.3. Control Barrier Function

This subsection presents the design of the control barrier function (CBF) and its role in ensuring system safety. The overall closed-loop configuration incorporating the CBF is illustrated in Fig. 3 [73]. Consider a dynamic system described by

$$\dot{x} = f(x) + g(x)\, u, \tag{15}$$

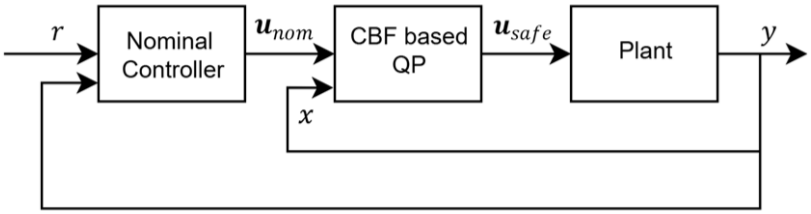

Fig. 3. Block diagram of the closed-loop system with CBF.

Where $x \in \mathbb{R}^n$ denotes the system state and $u \in \mathbb{R}^m$ is the control input. The functions $f : \mathbb{R}^n \to \mathbb{R}^n$ and $g : \mathbb{R}^n \to \mathbb{R}^{n \times m}$ are considered to maintain locally Lipschitz continuous. The control input $u : \mathbb{R}^n \to \mathbb{R}^m$ is also assumed to be locally Lipschitz continuous, ensuring that the closed-loop dynamics in (15) are well-defined. Under these assumptions, for any initial condition $x_0 \in \mathbb{R}^n$, there exists a maximal interval of existence $I(x_0) = [0, \tau_{\max})$ on which a unique solution $x : I(x_0) \to \mathbb{R}^n$ satisfies (15) with the initial state $x(0) = x_0$.

The concept of safety is formalized by defining a *safe set* within which the system state must remain to ensure safety. Specifically, consider a set $C \subset \mathbb{R}^n$ defined as the zero-superlevel set of a continuously differentiable function $h : \mathbb{R}^n \to \mathbb{R}$, where 0 is a regular value (i.e., $h(x) = 0 \implies \frac{\partial h}{\partial x}(x) \neq 0$). The safe set is thus given by

$$C \triangleq \{ x \in \mathbb{R}^n \mid h(x) \geq 0 \}. \tag{16}$$

We refer to C as the *safe set*, whose boundary and interior are respectively defined as

$$\partial C \triangleq \{ x \in \mathbb{R}^n \mid h(x) = 0 \},$$
$$\text{int}(C) \triangleq \{ x \in \mathbb{R}^n \mid h(x) > 0 \}.$$

CBF provides a constructive framework for synthesizing controllers which guarantee the forward invariance of a prescribed safe set, thereby ensuring the safety of the closed-loop system [42], [58]. Before formally defining CBFs, we first recall the following terminology. A continuous function $\alpha : (-b, a) \to \mathbb{R}$ is called an *extended class-$\mathcal{K}$* function ($\alpha \in \mathcal{K}_e$) if $\alpha(0) = 0$ and α is strictly

monotonically increasing. If $a = b = \infty$, $\lim_{r\to\infty} \alpha(r) = \infty$, and $\lim_{r\to-\infty} \alpha(r) = -\infty$, then α is said to be an *extended class-$\mathcal{K}_\infty$* function ($\alpha \in \mathcal{K}_{\infty,e}$).

This leads to the following definition of CBF. Safety is characterized by a safe set $C \subset \mathbb{R}^n$. Let $h : \mathbb{R}^n \to \mathbb{R}$ be a continuously differentiable function defining the boundary of C.

Definition 1 (Control Barrier Function, CBF) [58]. Let $C \subset \mathbb{R}^n$ be the zero-superlevel set of a continuously differentiable function $h : \mathbb{R}^n \to \mathbb{R}$, where 0 is a regular value. The function h is a CBF for the system in (15) on C if there exists $\alpha \in \mathcal{K}_{\infty,e}$ such that, for all $x \in C$,

$$\sup_{u\in\mathbb{R}^m} \Big[L_f h(x) + L_g h(x)\, u \Big] \;\geq\; -\alpha\big(h(x)\big), \tag{17}$$

Where $L_f h(x)$ and $L_g h(x)$ denote the Lie derivatives of h along $f(x)$ and $g(x)$, respectively. This condition yields the *CBF control set*

$$U_{\text{cbf}}(x) = \Big\{ u \in \mathbb{R}^m \;\Big|\; L_f h(x) + L_g h(x)\, u + \alpha\big(h(x)\big) \geq 0 \Big\}, \tag{18}$$

Which contains all admissible control inputs ensuring that the state trajectory remains within the safe set C for all time.

Definition 2 (Exponential Control Barrier Function, CBF) [67] To overcome the relative-degree limitation of standard CBFs, the exponential CBF (eCBF) was introduced in [67]. When the safety function $h(x)$ has relative degree $r \geq 1$ (particularly $r > 1$), its r-th time derivative can be expressed as

$$h^{(r)}(x,u) = L_f^r h(x) + L_g L_f^{r-1} h(x)\, u, \tag{19}$$

Where $L_g L_f h(x) = L_g L_f^2 h(x) = \cdots = L_g L_f^{r-2} h(x) = 0$ and $L_g L_f^{r-1} h(x) \neq 0$. The augmented state variable η_h is defined as

$$\eta_h(x) := \begin{bmatrix} h(x) \\ \dot{h}(x) \\ \ddot{h}(x) \\ \vdots \\ h^{(r-1)}(x) \end{bmatrix} = \begin{bmatrix} h(x) \\ L_f h(x) \\ L_f^2 h(x) \\ \vdots \\ L_f^{r-1} h(x) \end{bmatrix}, \tag{20}$$

and the new scalar control input is defined as $\mu_h = L_f^r h(x) + L_g L_f^{r-1} h(x)\, u$. Hence, the dynamics of $h(x)$ can be reformulated as a linear system of the form

$$\begin{aligned} \dot{\eta}_h(x) &= F_h\, \eta_h(x) + B_h\, \mu_h, \\ h(x) &= C_h\, \eta_h(x), \end{aligned} \tag{21}$$

Where

$$F_h = \begin{bmatrix} 0 & 1 & 0 & \cdots & 0 \\ 0 & 0 & 1 & \cdots & 0 \\ \vdots & \vdots & \ddots & \ddots & \vdots \\ 0 & 0 & 0 & \cdots & 1 \\ 0 & 0 & 0 & \cdots & 0 \end{bmatrix}, \qquad B_h = \begin{bmatrix} 0 \\ 0 \\ \vdots \\ 0 \\ 1 \end{bmatrix}, \qquad C_h = \begin{bmatrix} 1 & 0 & \cdots & 0 \end{bmatrix}. \tag{22}$$

To drive the output $h(x)$ to zero, the pole-placement technique is employed to design a feedback law $\mu_h = -K_h\, \eta_h$ such that all closed-loop poles $p_h = -[p_1\; p_2\; \cdots\; p_{r_h}]$ satisfy $p_i \geq 0$, $i = 1, \ldots, r_h$. This yields $h(x(t)) = C_h e^{A_h t} \eta_h(x_0)$ with $A_h = F_h - B_h K_h$. It follows that $h(x(t)) \geq C_h e^{A_h t} \eta_h(x_0)$ if $\mu_h \geq -K_h \eta_h$.

For a safety set C characterized by an r-times continuously differentiable function $h(x)$, the function $h(x)$ is called an exponential CBF if there exists a row vector $K_h = [\, k_1 \; k_2 \; \cdots \; k_r \,]$ such that

$$\sup_{u \in \mathcal{U}} \left[L_f^r h(x) + L_g L_f^{r-1} h(x)\, u \right] \geq - K_h\, \eta_h(x). \tag{23}$$

Consequently, $h(x(t)) \geq C_h e^{A_h t} \eta_h(x_0) \geq 0$ whenever $h(x(0)) \geq 0$, ensuring forward invariance of the safe set C. An appropriate selection of K_h not only guarantees that A_h is Hurwitz (all eigenvalues have strictly negative real parts) but also ensures a dependence on the initial condition $\eta_h(x_0)$ that helps maintain forward invariance. The characteristic polynomial of A_h is expressed as

$$\lambda^r + k_r \lambda^{r-1} + \cdots + k_2 \lambda + k_1 = 0, \tag{24}$$

With corresponding poles $p_1, p_2, \ldots, p_r$.

A sequence of functions $y_i : \mathbb{R}^n \to \mathbb{R}$, each defining a superlevel set C_i, for $i = 1, 2, \ldots, r$, is introduced as

$$\begin{aligned} y_0(x) &= h(x), & C_0 &= \{ x : \; y_0(x) \geq 0 \}, \\ y_1(x) &= \dot{y}_0(x) + p_1 y_0(x), & C_1 &= \{ x : \; y_1(x) \geq 0 \}, \\ &\vdots & &\vdots \\ y_r(x) &= \dot{y}_{r-1}(x) + p_r y_{r-1}(x), & C_r &= \{ x : \; y_r(x) \geq 0 \}, \end{aligned} \tag{25}$$

With C_0 coinciding with C. Following the main result in [67], if C_i is forward invariant, then C_{i-1} is also forward invariant provided that $x_0 \in C_i \cap C_{i-1}$ and $p_i \geq 0$ for all $i = 1, \ldots, r$. From (25), if $x_0 \in C_i$, the following inequality holds:

$$\dot{y}_{i-1}\big(x(t)\big) + p_i\, y_{i-1}\big(x(t)\big) \geq 0. \tag{26}$$

Finally, the exponential CBF-based controller adopted in this study is formulated as the following quadratic program:

$$\begin{aligned} u(x) = \arg\min_{u \in \mathbb{R}^m} \; & \tfrac{1}{2} \, \| u - u_{\text{nom}} \|^2 \\ \text{s.t.} \quad & L_f^r h(x) + L_g \, L_f^{r-1} h(x)\, u + K_h \, \eta_h(x) \geq 0, \end{aligned} \tag{27}$$

Where u_{nom} denotes the nominal control input and the inequality constraint ensures satisfaction of the exponential CBF condition.

2.4. Proposed RC-CBF System

In this subsection, Table 1 provides an overview of the procedure for constructing the output-feedback RC integrated with CBF, as summarized in Table 1. The overall closed-loop structure of the RC–CBF system is illustrated in Fig. 4. In the proposed architecture, the nominal controller responsible for achieving high tracking accuracy is provided by the RCPD, which is designed solely to minimize the periodic tracking error in the unconstrained setting.

The CBF is not intended to improve tracking performance; instead, it is introduced as a supervisory safety layer that monitors the system state and ensures that the transient response remains confined within prescribed state and input bounds. Whenever the nominal RC–PD command would drive the system close to or beyond these safety limits, the CBF modifies this command through the QP so that the applied input satisfies the constraints while deviating as little as possible from the nominal control signal. The control strategy is then applied to a servo system model.

To ensure the performance advantages of the proposed method, we examine its robustness to disturbance and its capability to maintain both stability and safety. The systems performance is assessed using Max Error, RMSE, and overshoot, followed by further analysis, as detailed in Section 3. A summary of the research methodology is illustrated in the flowchart shown in Fig. 5.

Table 1. Design algorithm for RC–CBF system

RC–CBF System Design Steps
Step 1. Obtain the transfer function as given in (3) and the corresponding state-space model as in (5).
Step 2. Obtain the period of the periodic reference signal, T_r, to compute N for the design of the RC internal model.
Step 3. Determine the Q-filter $Q(z)$ using the expressions in (9) and (10).
Step 4. Design the internal model $I(z)$ according to (8).
Step 5. Determine the conventional controller $C(z)$ to result in a stable $P_s(z)$.
Step 6. Calculate the closed-loop plant model $P_s(z)$ based on (11).
Step 7. Design compensator $L(z)$ according to (13).
Step 8. Define the safety set C using the barrier function formulation in (16).
Step 9. Compute the Lie derivatives of the barrier function according to (17).
Step 10. Determine the relative degree r of $h(x)$ with respect to the system dynamics in (15), and if $r \geq 1$, construct the exponential CBF according to (19).
Step 11. Define the exponential CBF output equations according to (25)–(26), which yield affine-in-input inequality constraints.
Step 12. Formulate the CBF–QP–based controller as in (27), where the objective minimizes the deviation from the nominal control input while enforcing the exponential CBF constraints introduced earlier.
Step 13. Construct the RC-CBF system based on Fig. 4.

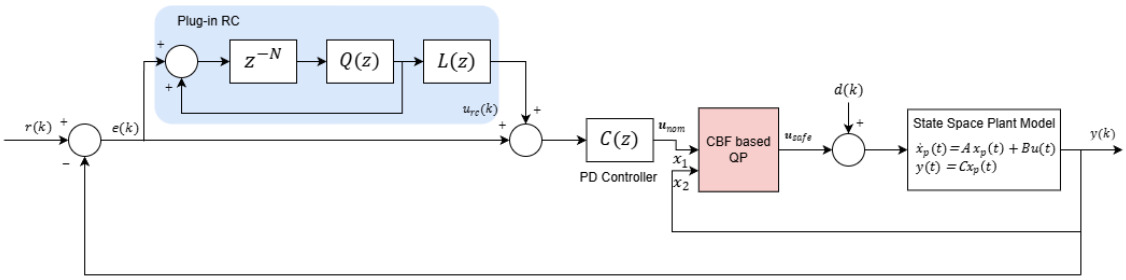

Fig. 4. Closed-loop structure of the RC–CBF system

3. Results and Discussion

3.1. Controller Design Parameters

To demonstrate the effectiveness of the proposed RC–CBF scheme, the control strategy is implemented on a Quanser SRV02 rotary servo system [74]. The servo parameters K and τ are obtained from frequency-response identification of the same servomotor hardware [74], yielding ($K = 1.74$) and ($\tau = 0.0268$). Using these values, the plant dynamics given by the second-order transfer function in (3) can be written as

$$P(s) = \frac{\theta(s)}{V_m(s)} = \frac{1.74}{s\,(0.0268\,s + 1)}, \tag{28}$$

Where $\theta(s)$ denotes the angular position (rad) and $V_m(s)$ represents the applied input voltage (V). Based on the state-space model (5), the parameters constructing system and input matrices are given by $-\frac{1}{\tau} = -37.3134$ and $\frac{K}{\tau} = 64.9254$. The plant model (28) is discretized using the zero-order-hold (ZOH) method with a sampling period of $T_s = 0.005$ s, yielding the following discrete-time state-space representation:

$$\begin{aligned} x[k+1] &= A_d\,x[k] + B_d\,u[k], \\ y[k] &= C\,x[k] + D\,u[k], \end{aligned} \tag{29}$$

Where

$$A_d = \begin{bmatrix} 1 & 0.0045613 \\ 0 & 0.8298 \end{bmatrix}, \quad B_d = \begin{bmatrix} 0.00076337 \\ 0.29614 \end{bmatrix}, \quad C = \begin{bmatrix} 1 & 0 \end{bmatrix}, \quad D = 0. \tag{30}$$

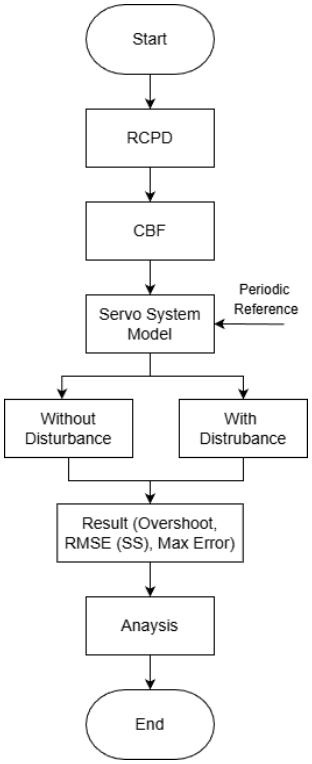

Fig. 5. Flowchart of research methodology

Meanwhile, the discrete-time transfer function of the model (28) is given by:

$$P(z) = \frac{0.0007634\,(z+0.9398)}{(z-1)\,(z-0.8285)}. \tag{31}$$

The resulting discrete-time plant (31) is marginally stable since one of its poles lies on the unit circle. To enhance the stability margin of the system, a conventional proportional–derivative (PD) controller $C(z)$ is incorporated, as indicated in (11), with proportional and derivative gains set to $K_p = 39.125$ and $K_d = 0.97813$, respectively. Consequently, the closed-loop plant model $P_s(z)$ can be expressed as

$$P_s(z) = \frac{0.17924\,(z+0.9397)\,(z-0.833)}{(z-0.8355)\,(z-(0.408-j0.0431))(z-(0.408+j0.0431))}. \tag{32}$$

We now obtain a third-order discrete-time closed-loop model as shown in (32), which has a relative degree of one. The closed-loop plant model $P_s(z)$ possesses three stable poles located at $p_1 = 0.408 + j0.0431$, $p_2 = 0.408 - j0.0431$, and $p_3 = 0.836$. According to (13), the compensator $L(z)$ is determined as

$$L(z) = \frac{(z-0.8355)\,\left(z^2-0.815\,z+0.1679\right)}{0.17924\,(z+0.9397)\,(z-0.833)}. \tag{33}$$

It is observed that $L(z)$ is an improper transfer function. However, it remains realizable since it can be rendered proper by multiplication with the term z^{-N} in the internal model $I(z)$. The periodic reference signal $r(k)$, with a maximum amplitude of 1.134 rad (65°) and a period of 2 s, is illustrated in Fig. 6. In the numerical simulation, a repetitive tracking control problem with external periodic disturbance is considered and ilustrated in Fig. 7. From Fig. 6, it can be observed that the reference signal has a period of $T_r = 2$ s, corresponding to a fundamental frequency of $f_r = 0.5$ Hz.

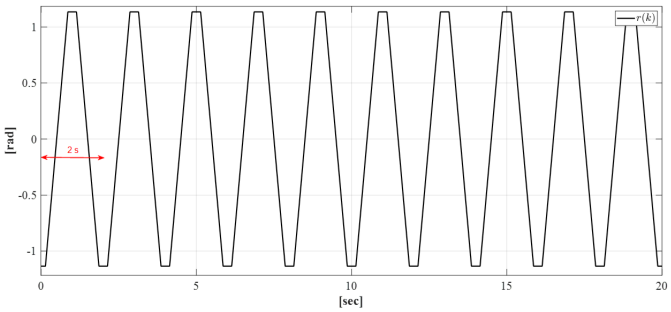

Fig. 6. Periodic reference signal $r(k)$

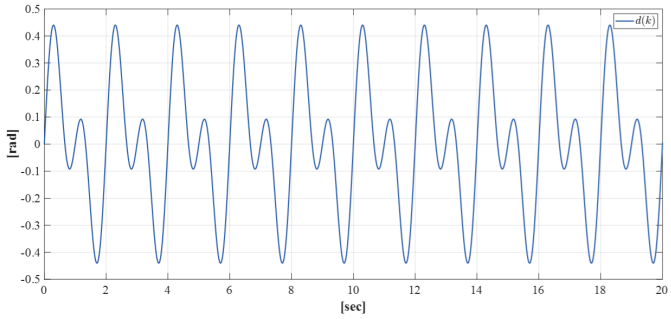

Fig. 7. Periodic disturbance signal $d(k)$

Hence, the delay length N used in constructing the internal model (8) is determined as $N = T_r/T_s = 2/0.005 = 400$. Furthermore, Fig. 7 shows the disturbance signal used in this study, which is defined as $d(k) = 0.25\sin(\pi t) + 0.25\sin(2\pi t)$. The Q-filter is chosen as

$$Q(z) = 0.25z^{-1} + 0.5 + 0.25z, \tag{34}$$

Which represents zero-phase low-pass filter giving a unity gain (0 dB) with a tracking bandwidth of $f_c = 36.35$ Hz, which is sufficiently higher than the frequency content of the reference and disturbance signals; this ensures that the RC retains adequate tracking accuracy and removes unnecessary high-frequency components, as shown in Fig. 8. In addition, the filter contributes zero phase to the RC system.

By substituting into (7), the transfer function of the output-feedback RC can be expressed as

$$\frac{U_{rc}(z)}{E(z)} = \frac{(0.25\,z^{-1} + 0.5 + 0.25\,z)\,z^{-400}}{1 - (0.25\,z^{-1} + 0.5 + 0.25\,z)\,z^{-400}} \left[\frac{(z - 0.8355)\,(z^2 - 0.815\,z + 0.1679)}{0.17924\,(z + 0.9397)\,(z - 0.833)}\right]. \tag{35}$$

Next, we define the barrier functions with respect to the state variable x_1 as

$$\underbrace{h_1(x) = \theta_{\max} - x_1}_{\text{Upper barrier}} \;;\; \underbrace{h_2(x) = x_1 + \theta_{\max}}_{\text{Lower barrier}}, \tag{36}$$

Which correspond to the upper and lower position constraints of the servomotor shaft, respectively.

The gradients of the barrier functions, $\nabla h_{1,2}(x) \in \mathbb{R}^{2\times 1}$, are obtained by taking the partial derivatives of $h_{1,2}(x)$ with respect to the state vector $\mathbf{x} = \begin{bmatrix} x_1 & x_2 \end{bmatrix}^\top$. For (36), the resulting gradients are

$$\nabla h_1(x) = \begin{bmatrix} -1 \\ 0 \end{bmatrix}, \qquad \nabla h_2(x) = \begin{bmatrix} 1 \\ 0 \end{bmatrix}. \tag{37}$$

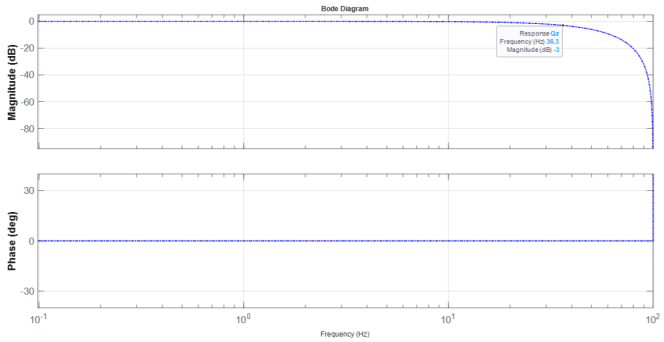

Fig. 8. Magnitude and phase responses of $Q(z)$.

Using the servomotor plant model in state-space form (5), the drift and input vector fields are expressed as

$$f(x) = \begin{bmatrix} x_2 \\ 1 \\ -\frac{1}{\tau}x_2 \end{bmatrix}, \qquad g(x) = \begin{bmatrix} 0 \\ \frac{K}{\tau} \end{bmatrix}. \tag{38}$$

To characterize the rate of change of each barrier function $h_{1,2}(x)$ under the system dynamics, the corresponding Lie derivatives with respect to the drift and input vector fields are computed as

$$\begin{aligned} L_f h_{1,2}(x) &= \nabla h(x)^\top f(x), \\ L_g h_{1,2}(x) &= \nabla h(x)^\top g(x). \end{aligned} \tag{39}$$

Consequently, we obtain $L_f h_1(x) = -x_2$ and $L_g h_1(x) = 0$, whereas for $h_2(x)$ we have $L_f h_2(x) = x_2$ and $L_g h_2(x) = 0$. Since the plant exhibits a relative degree greater than or equal to one ($r \geq 1$) with respect to the barrier function $h(x)$, the exponential CBF framework is adopted. By invoking (19), we take the second time derivative of $h(x)$ to obtain

$$h^{(2)}(x,u) = L_f^2 h(x) + L_g L_f h(x)\, u, \tag{40}$$

Where $L_f^2 h(x)$ denotes the Lie derivative of $h(x)$ taken twice along the drift field f, and $L_g L_f h(x)$ is the Lie derivative taken first along f and then along the input field g.

To evaluate $L_g L_f h_{1,2}(x)$, we differentiate $L_f h_{1,2}(x)$ with respect to the state vector $x = \begin{bmatrix} x_1 & x_2 \end{bmatrix}^\top$ to obtain the required gradients. From the previously obtained expressions, $\nabla\big(L_f h_1(x)\big) = \begin{bmatrix} 0 \\ -1 \end{bmatrix}$ and $\nabla\big(L_f h_2(x)\big) = \begin{bmatrix} 0 \\ 1 \end{bmatrix}$. The Lie derivative with respect to the input field g is then given by

$$L_g L_f h_{1,2}(x) = \nabla\big(L_f h_{1,2}(x)\big)^\top g(x), \tag{41}$$

From which we obtain $L_g L_f h_1(x) = -K/\tau$ and $L_g L_f h_2(x) = K/\tau$. The second Lie derivative along the drift field is computed as $L_f^2 h_{1,2}(x) = \nabla\big(L_f h_{1,2}(x)\big)^\top f(x)$, yielding $L_f^2 h_1(x) = \frac{1}{\tau}x_2$ and $L_f^2 h_2(x) = -\frac{1}{\tau}x_2$.

The auxiliary system (F_h, B_h) in (22) is assigned repeated real poles $s = -\lambda$ with $\lambda > 0$, which corresponds to choosing $p_1 = p_2 = \lambda$ in the operator $\left(\frac{d}{dt} + p_i\right)$. Using (25), the general output relation is expressed as

$$y_i(x) = \left(\frac{d}{dt} + p_1\right) \circ \left(\frac{d}{dt} + p_2\right) \circ \cdots \circ \left(\frac{d}{dt} + p_r\right) h(x), \quad i = 1, \ldots, r. \tag{42}$$

In particular, $y_1(x) = \left(\frac{d}{dt} + p_1\right)h(x)$ and $y_2(x) = \left(\frac{d}{dt} + p_2\right)y_1(x)$, which gives

$$y_2(x) = \ddot{h}(x) + (p_1 + p_2)\dot{h}(x) + p_1 p_2\, h(x). \tag{43}$$

Assuming repeated real pole placement with $p_1 = p_2 = \lambda > 0$, we have $p_1 + p_2 = 2\lambda$ and $p_1 p_2 = \lambda^2$. Hence,

$$y_2(x) = \ddot{h}(x) + 2\lambda\, \dot{h}(x) + \lambda^2 h(x) \geq 0. \tag{44}$$

The parameter $\lambda > 0$ is a design constant chosen such that the operator $\left(\frac{d}{dt} + \lambda\right)^2$ is Hurwitz, ensuring exponential convergence of the auxiliary dynamics. This yields the feedback gain $K_h = [\lambda^2 \;\; 2\lambda]$.

Substituting (40) into (44), we obtain

$$y_2(x) = L_f^2 h(x) + L_g L_f h(x)\, u + 2\lambda\, \dot{h}(x) + \lambda^2 h(x) \geq 0. \tag{45}$$

By substituting the previously derived Lie derivatives into (45), the barrier functions $h_{1,2}(x)$ yield the following constraints:

Upper Barrier: for $h_1(x) = \theta_{\max} - x_1$,

$$L_f^2 h_1(x) + L_g L_f h_1(x)\, u + 2\lambda\, \dot{h}_1(x) + \lambda^2 h_1(x) \geq 0 \implies u \leq \frac{\tau}{K}\left(\frac{1}{\tau}x_2 - 2\lambda x_2 + \lambda^2(\theta_{\max} - x_1)\right). \tag{46}$$

Lower barrier: for $h_2(x) = x_1 + \theta_{\max}$,

$$L_f^2 h_2(x) + L_g L_f h_2(x)\, u + 2\lambda\, \dot{h}_2(x) + \lambda^2 h_2(x) \geq 0 \implies u \geq \frac{\tau}{K}\left(\frac{1}{\tau}x_2 - 2\lambda x_2 - \lambda^2(x_1 + \theta_{\max})\right). \tag{47}$$

Finally, by combining these conditions with (27), the exponential CBF-based QP controller is formulated as

$$\begin{aligned} u_{\text{safe}} &= \arg\min_{u \in \mathbb{R}^m} \tfrac{1}{2}\, \|u - u_{\text{nom}}\|^2 \\ \text{s.t. } & L_f^2 h_i(x) + L_g L_f h_i(x)\, u + 2\lambda\, \dot{h}_i(x) + \lambda^2 h_i(x) \geq 0, \quad i = 1, 2. \end{aligned} \tag{48}$$

The CBF-based safety filter is implemented as a quadratic program solved using MATLAB's quadprog with its default interior-point configuration. All numerical tolerances, feasibility recovery steps, and handling of constraint interactions rely on the solver's built-in mechanisms, which follow MATLAB's standard optimization procedures.

3.2. Results and Comparison Studies

By increasing the state constraint on the angular position to a value slightly higher than the maximum reference amplitude, i.e., $\theta_{\max} = 1.14$ rad (65.31°), the controller is allowed to utilize the full reference range while still limiting excessive excursions of the output. The tracking performance of the RC–CBF controller is evaluated using the design parameter $\lambda = 65$ and compared with other control schemes, namely RC, PD–CBF, and PD controllers.

The CBF parameter λ is selected by manual tuning and directly shapes the trade-off between safety conservatism and tracking performance. If λ is chosen too small, the CBF behaves overly conservatively, so that the nominal controller cannot drive the control signal to the desired peak amplitude of the reference, which degrades tracking accuracy. Conversely, if λ is chosen too large, the correction generated by the CBF becomes too aggressive, making the resulting control signal oscillatory and potentially destabilizing the response of the nominal controller. The value $\lambda = 65$ is

adopted in this study as a compromise that preserves stability while providing a satisfactory balance between safety enforcement and tracking performance.

The performance of the RC–CBF system is further analyzed through the tracking error plot shown in Fig. 11 and Fig. 13. For quantitative comparison, additional performance indices—namely percentage overshoot, maximum error, and the root-mean-square of the steady-state error (rms-ess)—are calculated. These metrics are defined as follows:

$$\%\text{Overshoot} = \frac{(\text{MaxOut} + |\text{MinOut}|) - 2\,A_{\text{mIn}}}{2\,A_{\text{mIn}}} \times 100\%, \tag{49}$$

Where MaxOut and MinOut represent the maximum and minimum values of the system output, respectively, and A_{mIn} denotes the amplitude of the periodic reference signal.

$$\text{rms-ess} = \sqrt{\frac{1}{N_{ss}} \sum_{k=1}^{N_{ss}} e^2(k)}, \tag{50}$$

Where t_{ss} denotes the time at which the controller reduces the tracking error to within 5% of the reference peak, N_{ss} is the number of samples in the steady-state interval, and $e(k)$ is the tracking error.

3.2.1. Tracking Performance Without Disturbance

The trajectory and output responses of the system under RC–CBF and the other control strategies without disturbance are illustrated in Fig. 9. As shown in Fig. 9, the RC–CBF effectively suppresses transient overshoot, whereas the RC without safety constraints exhibits a pronounced overshoot around $t = 2$ s.

Nevertheless, both RC-based approaches achieve accurate steady-state tracking of the periodic reference. In contrast, the PD–CBF controller produces minimal overshoot but fails to track the periodic reference accurately in steady state, thus compromising long-term tracking precision.

Fig. 10 compares the control inputs generated by RC and the proposed RC-CBF controller in steady-state operation. Both controllers produce a periodic control pattern synchronized with the reference, but the RC input exhibits sharp high-amplitude pulses, especially around the rising and falling edges of each cycle.

When the CBF is integrated into the RC loop, these peaks are noticeably reduced and the control signal remains confined within a tighter voltage range while preserving the overall shape required for accurate tracking.

The computed performance metrics for the RC–CBF and the other control schemes are summarized in Table 2. As shown in Table 2, RC achieves the smallest steady-state error, with an RMS-ESS of 0.0200°, but exhibits the poorest transient behavior, as reflected by a large maximum error of 51.1365° and an overshoot of 39.40%. When the CBF is integrated with RC, the transient response is dramatically improved: the overshoot is completely eliminated (0%) and the maximum error is reduced to 2.7788°. This improvement comes at the cost of an increase in steady-state error, from 0.0200° to 0.1547°. This increase is mainly due to the conservative position constraint, $\theta_{\max} = 1.14$ rad (65.31°), which is only slightly higher than the maximum reference amplitude.

As a result, the CBF-based QP remains mildly active near the peaks of the trajectory, clipping the nominal RC command and preventing the internal model from exactly reproducing the reference amplitude, so that a small residual steady-state error is preserved in each cycle.

At the same time, placing the safety boundary just above the reference peak ensures that any potential overshoot is completely removed and that the state trajectory never leaves the prescribed safe region, providing strict transient safety while incurring only a very small steady-state error.

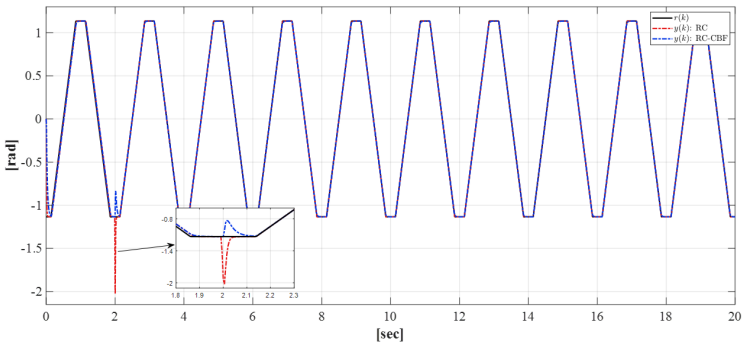

(a)

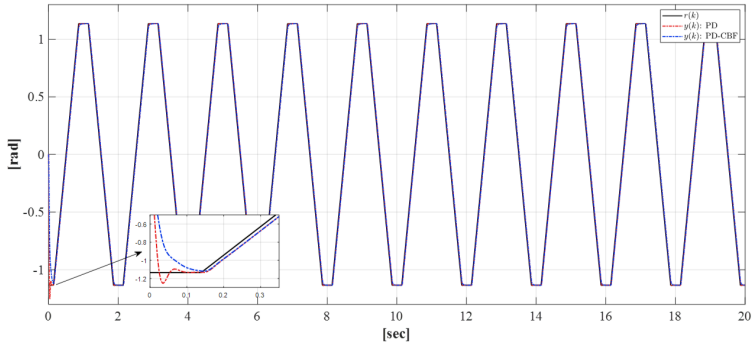

(b)

Fig. 9. **(a)** Tracking outputs of RC and RC-CBF **(b)** Tracking outputs of PD and PD-CBF Without Disturbance

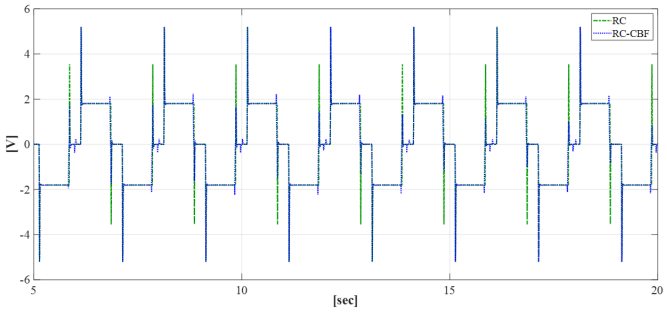

Fig. 10. Control signal of RC and RC-CBF

Table 2. Comparison of performance metrics for different controllers without disturbance

Method	Max Error (deg)	RMS-ESS (deg)	Overshoot (%)
RC	51.1365	0.0200	39.40
RC-CBF	2.7788	0.1547	0.00
PD	6.8870	2.2345	5.37
PD-CBF	2.7846	2.2460	0.00

In contrast, the PD controller suffers from severe overshoot (5.37%) and poor steady-state tracking, with an RMS-ESS of 2.2345°, indicating its inability to maintain accurate tracking of the periodic reference.

Although incorporating a CBF into the PD controller (PD-CBF) successfully eliminates the overshoot and limits the maximum deviation to 2.7846°, its steady-state accuracy remains inadequate, as shown by the RMS-ESS of 2.22460°.

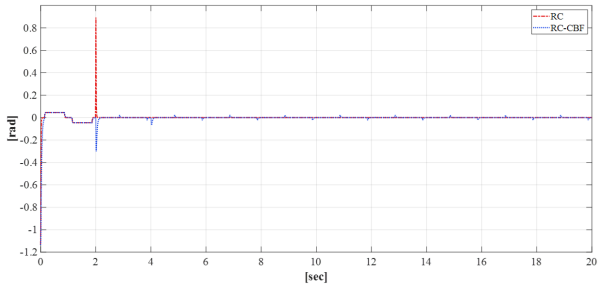

(a)

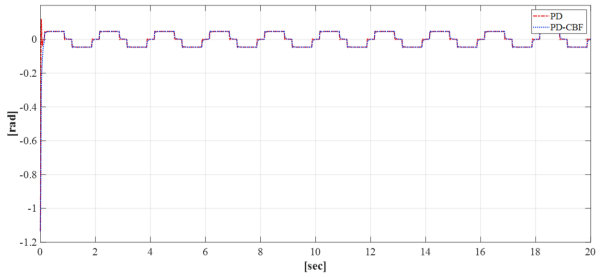

(b)

Fig. 11. **(a)** Tracking errors of RC and RC-CBF **(b)** tracking errors of PD and PD-CBF without disturbance

3.2.2. Tracking Performance With Disturbance

Fig. 12 shows the corresponding tracking responses in the presence of disturbance. The overall qualitative behavior is similar to the disturbance-free case: as seen in Fig. 12 (a), the RC-CBF still removes the transient overshoot exhibited by the conventional RC and keeps the trajectory within the prescribed bounds, while both RC-based controllers converge closely to the periodic reference in steady state.

Compared with the disturbance-free case in Table 2, the presence of disturbance slightly degrades the performance of all controllers, as evidenced by the increased overshoot and steady-state error values reported in Table 3.

From a robustness perspective, however, the RC-CBF exhibits the smallest degradation among the considered schemes: its maximum error increases only marginally (from 2.7788° to 2.8992°) and importantly, its overshoot remains identically zero even in the disturbed case. This indicates that the CBF layer effectively preserves the transient safety envelope in the presence of disturbance, while allowing the RC to maintain accurate periodic tracking.

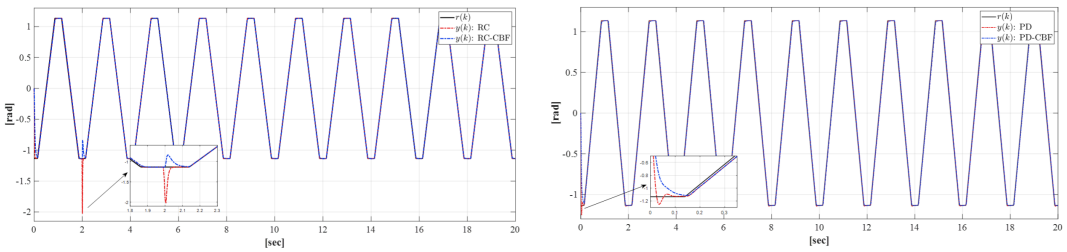

(a) (b)

Fig. 12. **(a)** Tracking outputs of RC and RC-CBF **(b)** Tracking outputs of PD and PD-CBF with distrubance

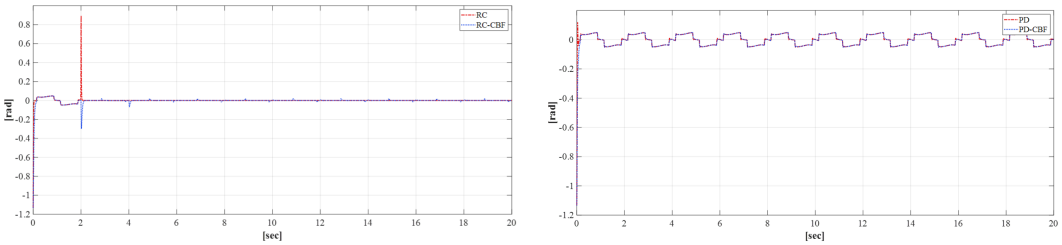

(a) (b)

Fig. 13. **(a)** Tracking errors of RC and RC-CBF **(b)** tracking errors of PD and PD-CBF with distrubance

Table 3. Comparison of performance metrics for different controllers with disturbance

Method	Max Error (deg)	RMS-ESS (deg)	Overshoot (%)
RC	51.2511	0.0204	39.53
RC-CBF	2.8992	0.1960	0.00
PD	6.8990	2.3914	5.39
PD-CBF	2.9039	2.6291	0.00

Overall, the RC-CBF still provides the most balanced trade-off between tracking performance and safety enforcement: it maintains precise periodic tracking with a small steady-state error while ensuring transient safety, whereas the conventional RC attains accuracy only at steady state, and PD-based controllers remain insufficiently accurate despite improved safety guarantees.

4. Conclusion

In this paper, an output-feedback Repetitive Control (RC) scheme integrated with a Control Barrier Function (CBF) has been developed for safe periodic tracking. The output-feedback RC component is employed to learn and compensate periodic reference and disturbance signals, while an exponential-type CBF is designed to enforce safety constraints on both the system states and control inputs via a quadratic-program-based safety filter. The effectiveness of the proposed RC-CBF framework has been validated through numerical simulations on a servomotor model, considering both disturbance-free and disturbance scenarios. The results show that integrating the CBF with RC does not preserve the original steady-state accuracy of the standalone RC but instead provides a systematic trade-off between steady-state tracking accuracy and transient safety. Compared with conventional RC, the RC-CBF controller completely eliminates overshoot and significantly reduces the maximum error, while incurring a slight increase in steady-state error. However, this steady-state error remains significantly small, so the loss in accuracy is negligible for the considered application compared with the substantial gains in transient safety. From a computational standpoint, the additional overhead introduced by the CBF-based QP remains modest in the present single-input servomotor case the resulting low-dimensional program can be solved well within the sampling interval on typical modern control hardware. Future research should focus on extending this approach to multivariable systems and performing real-time experimental validation on hardware platforms in realistic scenarios, together with a systematic evaluation of computational requirements, QP feasibility under model uncertainty, and robustness to a broader class of disturbances beyond the periodic cases considered in this study. These properties make the proposed RC-CBF framework particularly attractive for industrial machinery requiring active vibration compensation, where large transient overshoot and constraint violations cannot be tolerated.

Author Contribution: All authors contributed equally to this paper. All authors read and approved the final paper.

Funding: This research received no external funding.

Acknowledgment: The authors would like to thank Muhamad Rausyan Fikri from Tampere University for his valuable discussions and insightful comments regarding the Control Barrier Function (CBF) formulation.

Conflicts of Interest: The authors declare no conflict of interest.

References

[1] T. Inoue, M. Nakano, T. Kubo, S. Matsumoto, and H. Baba, "High Accuracy Control of a Proton Synchrotron Magnet Power Supply," *IFAC Proceedings*, vol. 14, no. 2, pp. 3137–3142, 1981, https://doi.org/10.1016/S1474-6670(17)63938-7.

[2] B. A. Francis and W. M. Wonham, "The internal model principle of control theory," *Automatica*, vol. 12, no. 5, pp. 457–465, 1976, https://doi.org/10.1016/0005-1098(76)90006-6.

[3] G. A. Ramos and R. Costa-Castelló, "Comparison of different repetitive control architectures: Synthesis and comparison. Application to VSI converters," *Electronics*, vol. 7, no. 12, p. 446, 2018, https://doi.org/10.3390/electronics7120446.

[4] G. Hillerström and K. Walgama, "Repetitive control theory and applications – A survey," *IFAC Proceedings Volumes*, vol. 29, no. 1, pp. 1446–1451, 1996, https://doi.org/10.1016/s1474-6670(17)57870-2.

[5] J. She, L. Zhou, M. Wu, J. Zhang, and Y. He, "Design of a modified repetitive-control system based on a continuous–discrete 2D model," *Automatica*, vol. 48, no. 5, pp. 844–850, 2012, https://doi.org/10.1016/j.automatica.2012.02.019.

[6] E. Kurniawan, Z. Cao, and Z. Man, "Design of robust repetitive control with time-varying sampling periods," *IEEE Transactions on Industrial Electronics*, vol. 61, no. 6, pp. 2834–2841, 2014, https://doi.org/10.1109/tie.2013.2276033.

[7] H. Ren, X. Liu, Z. Zhang, R. Duan, and Y. Liu, "Higher-order repetitive control enhanced FES for wrist intention tremor suppression," *Intelligent Robotics and Applications*, pp. 30–43, 2025, https://doi.org/10.1007/978-981-96-0777-83.

[8] Z. Zhang, B. Chu, Y. Liu, and D. H. Owens, "FES based wrist tremor suppression using multi-periodic repetitive control," *IFAC-PapersOnLine*, vol. 53, no. 2, pp. 10135–10140, 2020, https://doi.org/10.1016/j.ifacol.2020.12.2739.

[9] Z. Zhang, B. Huo, Y. Liu, A. Dong, and H. Yu, "Active disturbance rejection control of wrist tremor suppression system with additional high-order repetitive control component," *IEEE/ASME Transactions on Mechatronics*, vol. 30, no. 4, pp. 2438–2449, 2025, https://doi.org/10.1109/tmech.2024.3450599.

[10] T. Fang and C. T. Freeman, "Multiple model switched repetitive control for tremor suppression," *Mechatronics*, vol. 110, p. 103392, 2025, https://doi.org/10.1016/j.mechatronics.2025.103392.

[11] W. Lu, W. Wang, K. Zhou, and Q. Fan, "General high-order selective harmonic repetitive control for PWM converters," *IEEE Journal of Emerging and Selected Topics in Power Electronics*, vol. 10, no. 1, pp. 1178–1191, 2022, https://doi.org/10.1109/jestpe.2021.3101857.

[12] G. Yadav, "Enhancing power quality and stability in grid-interactive electric vehicle chargers using advanced control strategies and disturbance compensation," *Engineering Research Express*, vol. 7, no. 3, p. 035321, 2025, https://doi.org/10.1088/2631-8695/adf038.

[13] H. M. A. Antunes, R. R. D. Piero, and S. M. Silva, "Application of repetitive control to grid-forming converters in centralized AC microgrids," *Energies*, vol. 18, no. 13, p. 3427, 2025, https://doi.org/10.3390/en18133427.

[14] P. Pal, R. K. Behera, and U. R. Muduli, "Feedforward repetitive approach to disturbance rejection in DAB converters for EV charging," *IEEE Transactions on Industrial Electronics*, vol. 72, no. 8, pp. 7861–7873, 2025, https://doi.org/10.1109/tie.2024.3519565.

[15] H. Lin, X. Guo, D. Chen, S. Wu, and G. Chen, "A frequency adaptive repetitive control for active power filter with 380V/75A SiC-inverter," *IEEE Transactions on Industry Applications*, vol. 58, no. 4, pp. 5469–5479, 2022, https://doi.org/10.1109/tia.2022.3176848.

[16] K. Umeda, Y. Jiang, H. Yokoi, and S. Togo, "Repetitive control of robotic joint with variable impedance utilizing agonist-antagonist muscle pair structure based on virtual trajectories," *IEEE Access*, vol. 13, pp. 16866–16878, 2025, https://doi.org/10.1109/access.2025.3532633.

[17] X. Wang, A. Wang, D. Wang, W. Wang, B. Liang, and Y. Qi, "Repetitive control scheme of robotic manipulators based on improved B-Spline function," *Complexity*, vol. 2021, no. 1, 2021, https://doi.org/10.1155/2021/6651105.

[18] J. Hu, H. Lai, Z. Chen, X. Ma, and B. Yao, "Desired compensation adaptive robust repetitive control of a multi-DoFs industrial robot," *ISA Transactions*, vol. 128, pp. 556–564, 2022, https://doi.org/10.1016/j.isatra.2021.10.002.

[19] E. Kurniawan, H. Adinanta, H. G. Harno, J. A. Prakosa, S. Suryadi, and P. Purwowibowo, "On the synthesis of a stable and causal compensator for discrete-time high-order repetitive control systems," *International Journal of Dynamics and Control*, vol. 9, no. 2, pp. 727–736, 2020, https://doi.org/10.1007/s40435-020-00695-y.

[20] Y. Lan, J. Zhao, and J. She, "Preview repetitive control with equivalent input disturbance for continuous-time linear systems," *IET Control Theory & Applications*, vol. 16, no. 1, pp. 125–138, 2021, https://doi.org/10.1049/cth2.12214.

[21] E. Kurniawan, H. G. Harno, and H. Adinanta, "High-order repetitive model reference control for linear systems with uncertain periodic references and disturbances," *International Journal of Systems Science*, vol. 53, no. 7, pp. 1456–1468, 2021, https://doi.org/10.1080/00207721.2021.2008545.

[22] K. Zhou, C. Tang, Y. Chen, B. Zhang, and W. Lu, "A generic multi-frequency repetitive control scheme for power converters," *IEEE Transactions on Industrial Electronics*, vol. 70, no. 12, pp. 12680–12688, 2023, https://doi.org/10.1109/tie.2023.3239855.

[23] R. L. McGrath and F. Sergi, "Using repetitive control to enhance force control during human–robot interaction in quasi-periodic tasks," *IEEE Transactions on Medical Robotics and Bionics*, vol. 5, no. 1, pp. 79–87, 2023, https://doi.org/10.1109/tmrb.2023.3237766.

[24] E. Kurniawan, H. Wang, J. A. Prakosa, P. Purwowibowo, and E. B. Pratiwi, "An improved repetitive controller with fractional time-delay for discrete-time linear systems: Synthesis and comparison study," *ISA Transactions*, vol. 146, pp. 511–527, 2024, https://doi.org/10.1016/j.isatra.2023.12.035.

[25] S. Tian, K.-Z. Liu, Y. Wang, C. Lu, J. She, and M. Wu, "Enhanced disturbance rejection approach for repetitive-control systems based on a novel loop-shaping design," *IEEE Transactions on Industrial Electronics*, pp. 1–10, 2025, https://doi.org/10.1109/tie.2025.3595988.

[26] E. Kurniawan *et al.*, "Discrete-time design of fractional delay-based repetitive controller with sliding mode approach for uncertain linear systems with multiple periodic signals," *Fractal and Fractional*, vol. 9, no. 1, p. 41, 2025, https://doi.org/10.3390/fractalfract9010041.

[27] J. Na, X. Ren, R. Costa-Castelló, and Y. Guo, "Repetitive control of servo systems with time delays," *Robotics and Autonomous Systems*, vol. 62, no. 3, pp. 319–329, 2014, https://doi.org/10.1016/j.robot.2013.09.010.

[28] Z. Li, W. Zhang, Y. Zhang, and X. Xu, "Robust repetitive control design and its application on linear servo systems," *International Journal of Precision Engineering and Manufacturing*, vol. 16, no. 1, pp. 21–29, 2015, https://doi.org/10.1007/s12541-015-0003-7.

[29] E. Kurniawan *et al.*, "Robust adaptive repetitive control for unknown linear systems with odd-harmonic periodic disturbances," *Science China Information Sciences*, vol. 65, no. 12, 2022, https://doi.org/10.1007/s11432-022-3561-2.

[30] Z. Cao, Y. Feng, X. Yu, and R. F. A. Khan, "Discrete-time sliding mode repetitive control for servo motor systems," *IEEE/ASME Transactions on Mechatronics*, pp. 1–12, 2025, https://doi.org/10.1109/tmech.2025.3561026.

[31] L. Zhou, J. She, X.-M. Zhang, and Z. Zhang, "Additive-State-Decomposition-Based Repetitive Control for a Class of Nonlinear Systems with Multiple Mismatched Disturbances," *IEEE Transactions on Industrial Electronics*, vol. 68, no. 12, pp. 12565–12574, 2021, https://doi.org/10.1109/tie.2020.3039221.

[32] D. Astolfi, S. Marx, and N. van de Wouw, "Repetitive control design based on forwarding for nonlinear minimum-phase systems," *Automatica*, vol. 129, p. 109671, 2021, https://doi.org/10.1016/j.automatica.2021.109671.

[33] D. Astolfi, "Output-feedback repetitive control for minimum-phase nonlinear systems with arbitrarily relative degree," *IFAC-PapersOnLine*, vol. 54, no. 14, pp. 464–469, 2021, https://doi.org/10.1016/j.ifacol.2021.10.398.

[34] S. Tian *et al.*, "Improving Performance of Repetitive Control for Nonlinear Systems via Improved Disturbance Compensation," *IEEE Transactions on Industrial Informatics*, vol. 21, no. 7, pp. 5592–5602, 2025, https://doi.org/10.1109/tii.2025.3556061.

[35] L. Blanken, S. Koekebakker, and T. Oomen, "Multivariable Repetitive Control: Decentralized Designs With Application to Continuous Media Flow Printing," *IEEE/ASME Transactions on Mechatronics*, vol. 25, no. 1, pp. 294–304, 2020, https://doi.org/10.1109/tmech.2019.2951609.

[36] G. A. Ramos, R. I. Ruget, and R. Costa-Castello, "Robust Repetitive Control of Power Inverters for Standalone Operation in DG Systems," *IEEE Transactions on Energy Conversion*, vol. 35, no. 1, pp. 237–247, 2020, https://doi.org/10.1109/tec.2019.2948900.

[37] Y. Wang, L. Zheng, H. Zhang, and W. X. Zheng, "Fuzzy Observer-Based Repetitive Tracking Control for Nonlinear Systems," *IEEE Transactions on Fuzzy Systems*, vol. 28, no. 10, pp. 2401–2415, 2020, https://doi.org/10.1109/tfuzz.2019.2936808.

[38] M. Tian, B. Wang, Y. Yu, Q. Dong, and D. Xu, "Discrete-Time Repetitive Control-Based ADRC for Current Loop Disturbances Suppression of PMSM Drives," *IEEE Transactions on Industrial Informatics*, vol. 18, no. 5, pp. 3138–3149, 2022, https://doi.org/10.1109/tii.2021.3107635.

[39] R. Dinkla, T. Oomen, S. P. Mulders, and J.-W. van Wingerden, "Data-enabled Predictive Repetitive Control," *2024 IEEE 63rd Conference on Decision and Control (CDC)*, pp. 6749–6754, 2024, https://doi.org/10.1109/cdc56724.2024.10886847.

[40] E. Kurniawan *et al.*, "Attitude tracking of a multivariable 3-DoF helicopter via decentralized repetitive control," *Journal of the Franklin Institute*, vol. 362, no. 10, p. 107737, 2025, https://doi.org/10.1016/j.jfranklin.2025.107737.

[41] H. Guo, F. Zhang, Q. Zhang, Y. Liu, T. Xiang, and J. Xing, "A combined fractional order repetitive controller and dynamic gain regulator for speed ripple suppression in PMSM drives," *Actuators*, vol. 13, no. 2, p. 73, 2024, https://doi.org/10.3390/act13020073.

[42] A. D. Ames, S. Coogan, M. Egerstedt, G. Notomista, K. Sreenath, and P. Tabuada, "Control barrier functions: Theory and applications," *2019 18th European Control Conference (ECC)*, pp. 3420–3431, 2019, https://doi.org/10.23919/ecc.2019.8796030.

[43] A. Armghan *et al.*, "Barrier function based adaptive sliding mode controller for a hybrid AC/DC microgrid involving multiple renewables," *Applied Sciences*, vol. 11, no. 18, p. 8672, 2021, https://doi.org/10.3390/app11188672.

[44] B. Li, S. Wen, Z. Yan, G. Wen, and T. Huang, "A survey on the control Lyapunov function and control barrier function for nonlinear-affine control systems," *IEEE/CAA Journal of Automatica Sinica*, vol. 10, no. 3, pp. 584–602, 2023, https://doi.org/10.1109/jas.2023.123075.

[45] A. Anand, K. Seel, V. Gjærum, A. Håkansson, H. Robinson, and A. Saad, "Safe learning for control using control Lyapunov functions and control barrier functions: A review," *Procedia Computer Science*, vol. 192, pp. 3987–3997, 2021, https://doi.org/10.1016/j.procs.2021.09.173.

[46] X. Liu, M. Zhang, Z. Chu, and E. Rogers, "A sphere region tracking control scheme for underwater vehicles," *IEEE Transactions on Vehicular Technology*, vol. 72, no. 8, pp. 9835–9844, 2023, https://doi.org/10.1109/tvt.2023.3257763.

[47] S. Heshmati-Alamdari, M. Sharifi, G. C. Karras, and G. K. Fourlas, "Control barrier function based visual servoing for mobile manipulator systems under functional limitations," *Robotics and Autonomous Systems*, vol. 182, p. 104813, 2024, https://doi.org/10.1016/j.robot.2024.104813.

[48] Z. Artstein, "Stabilization with relaxed controls," *Nonlinear Analysis: Theory, Methods & Applications*, vol. 7, no. 11, pp. 1163–1173, 1983, https://doi.org/10.1016/0362-546x(83)90049-4.

[49] M. Z. Romdlony and B. Jayawardhana, "Uniting Control Lyapunov and Control Barrier Functions," *53rd IEEE Conference on Decision and Control*, pp. 2293–2298, 2014, https://doi.org/10.1109/cdc.2014.7039737.

[50] B. Dai, P. Krishnamurthy, and F. Khorrami, "Learning a Better Control Barrier Function," *2022 IEEE 61st Conference on Decision and Control (CDC)*, 2022, https://doi.org/10.1109/cdc51059.2022.9993334.

[51] F. Ferraguti *et al.*, "Safety and Efficiency in Robotics: The Control Barrier Functions Approach," *IEEE Robotics & Automation Magazine*, vol. 29, no. 3, pp. 139–151, 2022, https://doi.org/10.1109/mra.2022.3174699.

[52] K. Garg *et al.*, "Advances in the Theory of Control Barrier Functions: Addressing practical challenges in safe control synthesis for autonomous and robotic systems," *Annual Reviews in Control*, vol. 57, p. 100945, 2024, https://doi.org/10.1016/j.arcontrol.2024.100945.

[53] E. Daş and J. W. Burdick, "Robust Control Barrier Functions Using Uncertainty Estimation With Application to Mobile Robots," *IEEE Transactions on Automatic Control*, vol. 70, no. 7, pp. 4766–4773, 2025, https://doi.org/10.1109/tac.2025.3538742.

[54] M. Yu, C. Yu, M.-M. Naddaf-Sh, D. Upadhyay, S. Gao, and C. Fan, "Efficient Motion Planning for Manipulators with Control Barrier Function-Induced Neural Controller," *2024 IEEE International Conference on Robotics and Automation (ICRA)*, pp. 14348–14355, 2024, https://doi.org/10.1109/icra57147.2024.10610785.

[55] J. Sun, J. Yang, and Z. Zeng, "Safety-Critical Control With Control Barrier Function Based on Disturbance Observer," *IEEE Transactions on Automatic Control*, vol. 69, no. 7, pp. 4750–4756, 2024, https://doi.org/10.1109/tac.2024.3352707.

[56] M. Maghenem, A. J. Taylor, A. D. Ames, and R. G. Sanfelice, "Adaptive Safety Using Control Barrier Functions and Hybrid Adaptation," *2021 American Control Conference (ACC)*, pp. 2418–2423, 2021, https://doi.org/10.23919/acc50511.2021.9482871.

[57] A. D. Ames, J. W. Grizzle, and P. Tabuada, "Control barrier function based quadratic programs with application to adaptive cruise control," *53rd IEEE Conference on Decision and Control*, pp. 6271–6278, 2014, https://doi.org/10.1109/cdc.2014.7040372.

[58] A. D. Ames, X. Xu, J. W. Grizzle, and P. Tabuada, "Control Barrier Function Based Quadratic Programs for Safety Critical Systems," *IEEE Transactions on Automatic Control*, vol. 62, no. 8, pp. 3861–3876, 2017, https://doi.org/10.1109/tac.2016.2638961.

[59] Q. Hou, H. Wang, C. H. T. Lee, and S. Ding, "Composite adaptive super-twisting sliding mode control using barrier function for PM motor drives toward electric aircraft applications," *IEEE Transactions on Power Electronics*, vol. 40, no. 11, pp. 16255–16264, 2025, https://doi.org/10.1109/tpel.2025.3587024.

[60] S. Mobayen, "Design of adaptive global barrier-function PID-type finite time tracking control method for uncertain systems," *IEEE Transactions on Systems, Man, and Cybernetics: Systems*, vol. 55, no. 5, pp. 3693–3706, 2025, https://doi.org/10.1109/tsmc.2025.3546801.

[61] X. Zhao and L. Wang, "Bounded control of PMLSM servo system based on fractional order barrier function adaptive super-twisting approach," *Control Engineering Practice*, vol. 154, p. 106131, 2025, https://doi.org/10.1016/j.conengprac.2024.106131.

[62] B. Dai, Z. Wang, J. Zhao, and S. Li, "Critical current-constrained continuous nonsingular terminal sliding mode control for PMSM based on control barrier function," *IEEE Transactions on Power Electronics*, vol. 40, no. 10, pp. 15093–15103, 2025, https://doi.org/10.1109/tpel.2025.3576340.

[63] A. J. Taylor, A. Singletary, Y. Yue, and A. D. Ames, "A control barrier perspective on episodic learning via projection-to-state safety," *IEEE Control Systems Letters*, vol. 5, no. 3, pp. 1019–1024, 2021, https://doi.org/10.1109/lcsys.2020.3009082.

[64] T. G. Molnar, A. K. Kiss, A. D. Ames, and G. Orosz, "Safety-critical control with input delay in dynamic environment," *IEEE Transactions on Control Systems Technology*, vol. 31, no. 4, pp. 1507–1520, 2023, https://doi.org/10.1109/tcst.2022.3227451.

[65] R. K. Cosner, A. W. Singletary, A. J. Taylor, T. G. Molnar, K. L. Bouman, and A. D. Ames, "Measurement-robust control barrier functions: Certainty in safety with uncertainty in state," *2021 IEEE/RSJ International Conference on Intelligent Robots and Systems (IROS)*, pp. 6286–6291, 2021, https://doi.org/10.1109/iros51168.2021.9636584.

[66] B. Xu and K. Sreenath, "Safe teleoperation of dynamic UAVs through control barrier functions," *2018 IEEE International Conference on Robotics and Automation (ICRA)*, pp. 7848–7855, 2018, https://doi.org/10.1109/icra.2018.8463194.

[67] Q. Nguyen and K. Sreenath, "Exponential control barrier functions for enforcing high relative-degree safety-critical constraints," *2016 American Control Conference (ACC)*, pp. 322–328, 2016, https://doi.org/10.1109/acc.2016.75249355.

[68] W. Xiao and C. Belta, "High-order control barrier functions," *IEEE Transactions on Automatic Control*, vol. 67, no. 7, pp. 3655–3662, 2022, https://doi.org/10.1109/tac.2021.3105491.

[69] K. Shao, J. Zheng, R. Tang, X. Li, Z. Man, and B. Liang, "Barrier function based adaptive sliding mode control for uncertain systems with input saturation," *IEEE/ASME Transactions on Mechatronics*, vol. 27, no. 6, pp. 4258–4268, 2022, https://doi.org/10.1109/tmech.2022.3153670.

[70] S. Yan, L. Shi, H. Zhang, S. Yao, and Y. Zhou, "Safety-critical model-free adaptive iterative learning control for multi-agent consensus using control barrier functions," *IEEE Transactions on Circuits and Systems II: Express Briefs*, vol. 71, no. 1, pp. 221–225, 2024, https://doi.org/10.1109/tcsii.2023.3300978.

[71] A. A. H. Newaz and R. Jahan, "Comprehensive Dynamic Modeling of a Rotary Servo Base Unit Using Frequency Response and Bump Test Techniques," *American Journal of Mechanical Engineering*, vol. 13, no. 1, pp. 6–10, 2025, https://doi.org/10.12691/ajme-13-1-2.

[72] M. Tomizuka, T.-C. Tsao, and K.-K. Chew, "Analysis and synthesis of discrete-time repetitive controllers," *Journal of Dynamic Systems, Measurement, and Control*, vol. 111, no. 3, pp. 353–358, 1989, https://doi.org/10.1115/1.3153060.

[73] W. Shaw Cortez, D. Oetomo, C. Manzie, and P. Choong, "Control barrier functions for mechanical systems: Theory and application to robotic grasping," *IEEE Transactions on Control Systems Technology*, vol. 29, no. 2, pp. 530–545, 2021, https://doi.org/10.1109/tcst.2019.2952317.

[74] E. Kurniawan, *Robust Repetitive Control and Applications*. Swinburne University of Technology, Melbourne, Australia, 2013, https://doi.org/10.25916/sut.26283661.v1.